Intermolecular Interactions between Cholecystokinin-8 and the Third Extracellular Loop of the Cholecystokinin A Receptor[†,‡]

Craig Giragossian[§] and Dale F. Mierke*[,§,||]

Department of Chemistry and Department of Molecular Pharmacology, Division of Biology & Medicine, Brown University, Providence, Rhode Island 02912

Received November 20, 2000; Revised Manuscript Received January 29, 2001

ABSTRACT: The interaction of the C-terminal octapeptide of cholecystokinin, CCK-8, with the third extracellular loop of human cholecystokinin-A receptor, CCK_A-R(329−357), has been probed by high-resolution NMR and extensive computer simulations. The structure of CCK_A-R(329−357) in the presence of dodecylphosphocholine micelles consists of three α-helices, with the first and third corresponding to the extracellular ends of transmembrane (TM) helices 6 and 7. The central helix, residues W335−R345, is found to lie on the zwitterionic surface. Titration with CCK-8 produces a stable complex with a number of intermolecular NOEs between the C-terminus of the ligand (Trp^{30}, Met^{31}, Asp^{32}) and the interface of TM6 and the third extracellular loop (N333, A334, Y338) of the receptor fragment. The mode of ligand binding based on these intermolecular NOEs is in agreement with a number of published findings from receptor mutagenesis and photoaffinity cross-linking. Utilizing these ligand/receptor points of interaction, the structural features of CCK_A-R(329−357), and also the structures of CCK-8 and CCK_A-R(1−47) previously determined, extensive molecular dynamics simulations of the CCK-8/CCK_A-R complex were carried out. The results provide unique insight into the molecular interactions and forces important for the binding of CCK-8 to CCK_A-R.

Cholecystokinin (CCK)[1] is a peptide hormone and neurotransmitter which activates two distinct G-protein-coupled receptor subtypes (CCK_A-R and CCK_B-R) (*1*). The CCK_A and CCK_B receptors are expressed in the gastrointestinal tract and central nervous system, respectively, and are characterized by seven hydrophobic transmembrane domains, an extracellular N-terminus, and an intracellular C-terminus. In the gastrointestinal tract, CCK is involved in a number of physiological processes including gall bladder contractions, pepsinogen secretion, pancreatic amylase secretion, inhibition of gastric emptying, and decreased small bowl and increased colonic transit times, whereas in the central nervous system CCK effectuates satiety, anxiety, memory, and analgesia (*1*−*5*). CCK is released into the blood and into the synaptic space of neurons in response to stimulation by nutriment in the gastrointestinal tract; therefore, the CCK_A receptor subtype is an attractive target for the development of pharmaceutically driven therapies for the treatment of obesity (*6*).

The active forms of cholecystokinin (e.g., CCK-58, CCK-33, and CCK-8) are processed from a 115 amino acid preprohormone in the rough endoplasmic reticulum and the golgi apparatus of GI cells and neurons (*3*). Affinity for CCK_A-R resides in the C-terminal octapeptide, Asp^{26}-Tyr-Met-Gly-Trp-Met-Asp-Phe^{33}-NH_2 (CCK-8), with the carboxyamidation of the C-terminal Phe^{33} residue quintessential for full biological activity (*5*). Sulfation of Tyr^{27} increases the affinity for the CCK_A-R, and therefore is often used to distinguish between functioning of CCK_A-R and CCK_B-R.

Over the years, efforts utilizing receptor mutagenesis and photoaffinity cross-linking have been carried out to probe the ligand/receptor complex. Site-directed mutagenesis-based studies have been used to determine specific points of contact between amino acid residues of CCK and the proximal N-terminus (*7*), second extracellular loop (*8*, *9*), and third extracellular loop of human CCK_A-R (*10*). Using photolabile analogues of CCK, intermolecular interactions with the ligand and the N-terminus (*11*) and third extracellular loop of rat CCK_A-R (*12*) have been reported. The results from these two methods differ with respect to the topological orientation of the ligand while bound to CCK_A-R. From site-directed mutagenesis and ligand truncation, the N-terminus of CCK-8 is found to interact with the N-terminus of CCK_A-R, whereas photoaffinity studies observe that the C-terminal residue, Phe^{33}, cross-links with the proximal N-terminus. In contrast to the results obtained with CCK_A-R, photoaffinity-based studies of the binding of CCK-8 to CCK_B-R place the

[†] This work was supported by the Research Foundation through a Cottrell Scholars Award (D.F.M.) and a Henry and Camille Dreyfus Scholars & Teachers Award (D.F.M.).

[‡] The structure coordinates have been deposited in the Brookhaven Protein Data Bank (filename 1HZN).

* To whom correspondence should be addressed at the Department of Molecular Pharmacology, Division of Biology & Medicine, Brown University, Providence, RI 02912. Voice: (401) 863-2139, Fax: (401) 863-1595, E-mail: Dale_Mierke@Brown.edu.

[§] Department of Chemistry.

[||] Department of Molecular Pharmacology.

[1] Abbreviations: Bpa, L-benzoylphenylalanine; CCK, cholecystokinin; CCK_A-R, cholecystokinin type A receptor; CCK_B-R, cholecystokinin type B receptor; DG, distance geometry; DPC, dodecylphosphocholine; EC, extracellular loop; G-protein, guanine nucleotide-binding regulatory protein; MD, molecular dynamics; NMR, nuclear magnetic resonance; NOE, nuclear Overhauser enhancement; NOESY, nuclear Overhauser enhancement spectroscopy; RMSD, root-mean-square deviation; TM, transmembrane; TOCSY, total-correlation spectroscopy.

10.1021/bi002659n CCC: $20.00
Published on Web 03/06/2001

N-terminus of the hormone in close proximity to the N-terminus of the receptor (*13*).

Recently, the structure of the N-terminus of human CCK_A-R(1−47) and its interactions with CCK-8 were reported (*14*). Intermolecular NOEs were observed between the N-terminal residues of CCK-8 (Tyr^{27} and Met^{28}) and W39 of the putative N-terminus of CCK_A-R.[2] These results were in complete accord with the findings from site-directed mutagenesis (*7*) and the cross-linking of CCK-8 to CCK_B-R (*13*).

In this study, we present the structure of the putative third extracellular loop of human CCK_A receptor, CCK_A-R(329−357), and its intermolecular contact points with CCK-8 as determined by solution NMR in the presence of zwitterionic lipids. The experimentally determined structures for CCK_A-R(1−47), CCK_A-R(329−357), and CCK-8 were incorporated into a molecular model of the entire receptor and subjected to extensive NOE-restrained molecular dynamics (MD) simulations. The NOE-derived contact points provide new insight into the intermolecular interactions involved in the binding of CCK-8 to the CCK_A receptor.

EXPERIMENTAL PROCEDURES

Peptide Synthesis. The receptor fragment CCK_A-R(329−357) was synthesized using solid-phase techniques at the Protein Chemistry Facility at Tufts University (Boston, MA). Purity and structural integrity were determined by liquid chromatography and mass spectrometry. NMR quantities of the receptor fragment were purified by semipreparative reverse-phase high-performance liquid chromatography. CCK-8 ($D^{26}YMGWMDF^{33}$-NH_2) was purchased from Phoenix Pharmaceutics Inc. (Mountain View, CA; purity ≥95%). Our previous results indicate that Tyr^{27} is interacting with the N-terminus of the CCK_A receptor, and therefore the nonsulfated form of CCK-8 should bind to the third extracellular loop in an identical fashion as the sulfated ligand. The nonsulfated CCK-8 is a full agonist of CCK_A, albeit with a reduced affinity, and therefore probably binds in an identical manner.

NMR Methods. Peptide solutions were prepared in water (90% H_2O/10% D_2O, Cambridge Isotopes) at a concentration of 2.5 mM peptide and 150 mM DPC-d_{38} (98.6%, Cambridge Isotopes). The final pH of the aqueous solution was 4.5 without correcting for the deuterium isotope effect. Proton NMR spectra were recorded on a Bruker Avance 600 MHz spectrometer and processed using NMRPipe (*15*). NOE cross-peaks were integrated using Felix (Molecular Simulations, Inc.).

Spin systems were assigned using TOCSY (*16*, *17*) and NOESY (*18*, *19*) spectra recorded in the phase-sensitive mode using the method from States (*20*) at 298−308 K with mixing times of 50−70 and 150 ms, respectively. The solvent signal was suppressed using the WATERGATE pulse sequence (*21*). The spectral width was 7500 Hz in both dimensions, with 2048 data points in f_2 and 512 data points in f_1, and 16−48 scans were collected at each increment.

Cross-peak volumes calculated from the NOESY spectra were converted to distances using the isolated two-spin approximation. Cross-peaks between the two β-methylene protons of W335 and P351 were used as an internal reference (1.8 Å). The calculated distances were then assigned to three classes based upon the NOE intensity: 1.8−3.0 (strong), 1.8−4.0 (medium), and 1.8−5.0 Å (weak). Pseudo atoms were used for protons that could not be stereospecifically assigned, and the upper distance restraints were corrected using standard procedures (*22*).

Structure Refinement. Metric matrix distance geometry (DG) calculations were carried out with a home-written program utilizing the random metrization algorithm of Havel (*23*). Experimental distance restraints that were more restrictive than the geometric distance bounds (holonomic restraints) were used to create the final distance matrix. The structures were embedded in four dimensions and refined following published procedures (*24*, *25*). The resulting structures were then reduced to three dimensions using metrization, and the optimization was repeated.

Molecular Dynamics of CCK_A-R(329−357). Molecular dynamics simulations of CCK_A-R(329−357) were performed using GROMACS v2.0 (*26*). A representative structure was selected from among the DG-generated structures and was placed in the center of a two-phase solvent box composed of water and decane ($x = y = z = 60$ Å). The aqueous and hydrophobic phases of the solvent box were filled with 2755 molecules of water and 495 molecules of decane, respectively. All ionizable functional groups were treated as charged species without the inclusion of counterions. Simulations were carried out with a time step of 1 fs and periodic boundary conditions. The neighbor list for nonbonded interactions was updated every 10 fs. The cutoff distance for Coulombic and nonbonded interactions was 10 Å. Distance restraints were applied with a force constant of 1000 kJ mol^{-1} nm^{-2}.

Molecular Modeling of the CCK_A Receptor. Transmembrane (TM) helices in the CCK_A-R were deduced by searching the amino acid sequence for long stretches of hydrophobic residues and by comparison to the amino acid sequence of other GPCRs (*27*, *28*). The initial positions of α carbons and side chains in the TM helices were modeled using the electron density map of rhodopsin (*29*) and WHATIF (*30*), respectively. The computationally refined NMR structures of the N-terminus and the third extracellular loop were directly incorporated into the model. A disulfide bond was created between C^{114} and C^{196}, in the first and second extracellular loops, respectively. The entire receptor was subjected to restrained energy minimization using steepest descent and conjugate gradients followed by template forcing of the TM helices to their initial positions (DISCOVER, MSI).

Molecular Dynamics of the CCK_A Receptor. The CCK_A receptor was placed in the center of a membrane-mimetic solvent box composed of decane sandwiched between two layers of water ($x = 100$ Å, $y = 90$ Å, $z = 90$ Å). The TM helices were placed in the decane phase, which extended 40 Å in the x dimension. The intracellular and extracellular components of the receptor were projected into the aqueous phases, each of which extended 30 Å in the x dimension. The aqueous and hydrophobic phases of the solvent box were filled with 14 839 and 673 molecules of water and decane, respectively. All other simulation parameters were the same as those used for the receptor fragment.

[2] To simplify the description of the interaction in the ligand/receptor complex, the amino acids of the ligand will be denoted using the three-letter code, while the one-letter code will be used for the residues of the receptor.

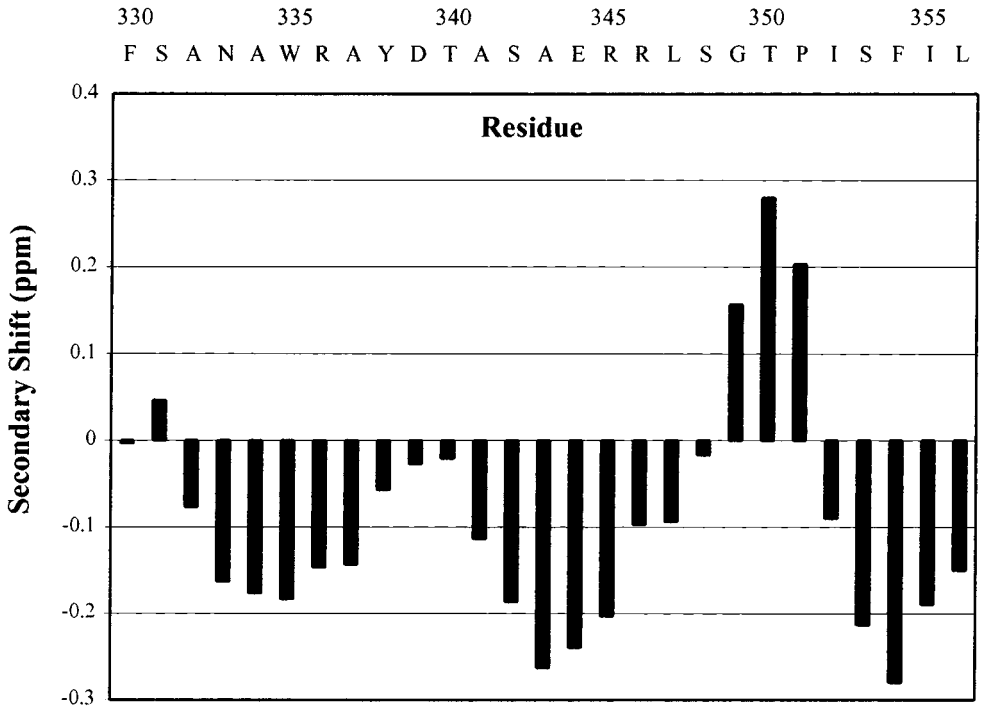

FIGURE 1: Hα secondary shifts for CCK_A-R(329−357). The chemical shifts were measured relative to TMS from a TOCSY spectrum collected at 35 °C with a mixing time of 50 ms.

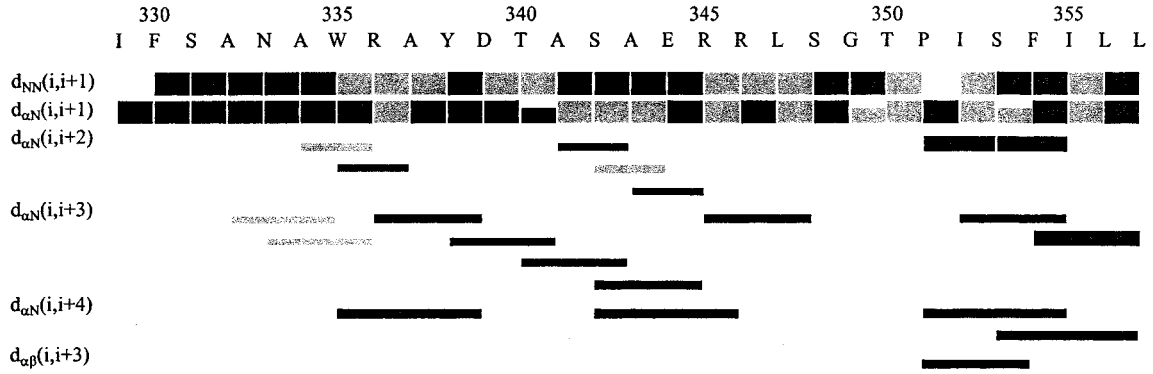

FIGURE 2: Structurally informative NOEs from the NOESY spectra collected at 298 and 308 K. The NOEs were classified as strong, medium, and weak according to the intensity of the integrated cross-peak volumes. Partially overlapped cross-peaks are depicted with shaded bars.

RESULTS

Structure of CCK_A-R(329−357). The receptor fragment examined here consists of the entire putative third extracellular loop and a few anchoring residues from the C-terminus and N-terminus of TM6 and TM7, respectively. Under the experimental conditions employed (a 1.2:1 ratio of micelle to receptor fragment, assuming 50 molecules of DPC per micelle), a single set of NMR signals was observed, indicating that CCK_A-R(329−357) associates with DPC micelles in a nonaggregated state (*31*). Association of the peptide with micelles of DPC was observed by an increase in the line width of the ^1H signals, as would be expected for a complex of this molecular weight. Diagnostic $H^{\alpha}_i/H^{\delta 1}_{i+1}$ and $H^{\alpha}_i/H^{\delta 2}_{i+1}$ cross-peaks between P351 and the preceding amino acid indicated that the amide bond was in the trans configuration. The presence of secondary structural elements was determined by analyzing the chemical shifts of the Cα protons. The secondary shift of the Hα of CCK_A-R(329−357) was consistent with helical elements in the N-terminal region between residues N333 and A337, the extracellular loop region between A341 and R345, and the C-terminal region between S353 and L356 (Figure 1).

A total of 220 distance restraints were generated from the NOESY spectra acquired at 298 and 308 K. Many of the structurally important NOEs are provided in Figure 2. The observed NOEs were generally consistent with the Hα secondary shift and provided evidence for helices in the N-terminal region between residues A332 and D339, the extracellular loop region between A341 and R346, and the C-terminal region between P351 and L356. The greatest disparity between the Hα secondary shift and the observed NOEs was observed for the N-terminus. However, the lack of αN(*i*,*i*+3) NOEs can be partially attributed to overlap in the NMR spectrum.

Metric-matrix DG calculations were utilized to search the conformational space of the receptor fragment, as allowed by the measured distance restraints. The resulting structures, all of which had distance violations lower than 0.2 Å,

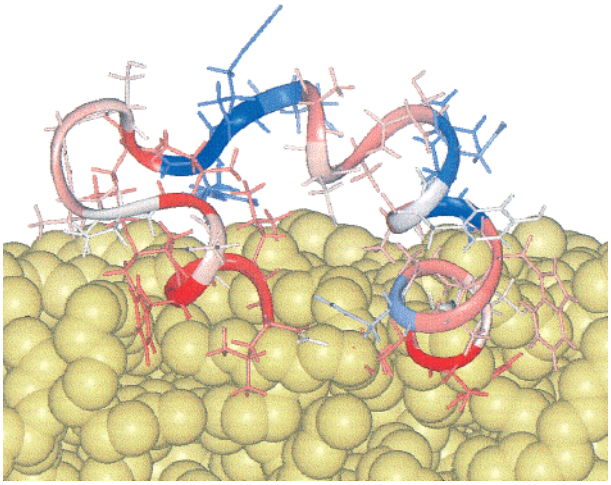

FIGURE 3: Structure of CCK$_A$-R(329−357) following an NOE-restrained MD simulation for 300 ps in a water/decane membrane-mimetic solvent box with periodic boundary conditions. The amino acids of the receptor fragment are color-coded according to hydrophobicity (blue = polar, red = hydrophobic), with TM 7 and TM 6 depicted on the left and right, respectively. The decane phase is depicted in gold CPK, and the water phase has been omitted for clarity.

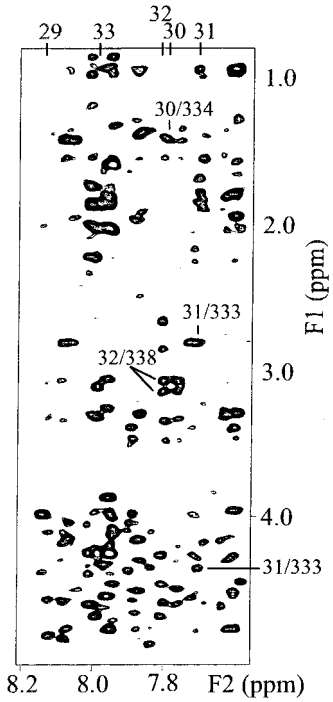

FIGURE 4: Expanded portion of the two-dimensional NOESY spectrum of the CCK-8/CCK$_A$-R(329−357) complex. The unambiguously assigned intermolecular NOEs are denoted, with the first number indicating the ligand (using the numbering of CCK-33).

displayed three distinct regions of helical character. A representative structure was selected and subjected to NOE-restrained MD simulations.

The CCK$_A$-R(329−357) receptor fragment was positioned in a decane/water solvent box with the hydrophobic residues of the N- and C-terminal helices partially embedded in the decane phase and with the hydrophilic residues of the extracellular loop projecting into the aqueous phase. During the MD simulation, the N-terminal helix became increasingly embedded in the hydrophobic phase, while the C-terminal helix did not move relative to the two phases. The extracellular loop of the receptor fragment was closely associated with the surface of the decane phase with the hydrophilic side chains extending into the aqueous phase (Figure 3). The three helices observed in the DG calculations were maintained throughout the entire MD simulation. During the last 50 ps of the simulation, the mean dihedral angles of the F330−A332, W335−S342, and I352−I355 residues were consistent with an α-helix, and the mean dihedral angles for the A343 and E344 residues were consistent with a 3_{10} helix. The mean distance constraint violations calculated at each time step of the simulation were less than 0.2 Å.

CCK$_A$-R(329−357)/CCK-8 Complex. Interactions between CCK-8 and CCK$_A$-R(329−357) were determined using 1D and 2D NMR. The ligand was added to the receptor fragment until the concentrations of the two peptides were equimolar, using the intensity of the indole NH resonances of Trp^{30} and W335 to monitor the effective concentration of CCK-8 and CCK$_A$-R(329−357), respectively. A number of unambiguous NOEs between the amide protons of the ligand and the Cα and Cβ protons of the receptor fragment were observed as illustrated in Figure 4. The contact points were localized in the C-terminus of CCK-8 and the N-terminus of the receptor fragment, corresponding to TM6 of CCK$_A$-R (Table 1).

To further characterize these interactions between CCK-8 and the third extracellular loop, a series of short (50 ps) NOE-restrained MD simulations were carried out. During these simulations, the intramolecular NOEs for CCK$_A$-R(329−357)

Table 1: Intermolecular NOEs Observed between CCK-8 and CCK$_A$-R(329−357)

ligand	receptor
Met^{31} hn	N333 α
Met^{31} hn	N333 β^a
Trp^{30} hn	A334 β^a
Asp^{32} hn	Y338 β1
Asp^{32} hn	Y338 β2

[a] Methylene/methyl protons are not resolved.

and CCK-8, as previously reported (*14*), and the ligand/receptor intermolecular distance restraints were applied. The simulations started with the ligand at different relative orientations and 10 Å removed from the receptor fragment. A number of these simulations converged to a similar low-energy structure fully consistent (less than 0.2 Å violation) with the intra- and intermolecular NOEs (the other simulations resulted in high-energy arrangements, with the structure of the ligand and/or receptor distorted). The resulting structure is shown in Figure 5. Specific interactions involve the side chains of Tyr^{27}, Trp^{30}, and Phe^{33} with A334, W335, and Y338. A hydrogen bond between the amide proton of Met^{31} and the carbonyl oxygen of N333 was observed during portions of the simulations.

Experimental Based Model of the CCK-8/CCK$_A$ Receptor Complex. To gain further insight into the intermolecular interactions between CCK-8 and CCK$_A$-R, the entire receptor was modeled using the α-carbon template of rhodopsin (*28*). The experimentally determined structures of the N-terminus, CCK$_A$-R(1−47), and the third extracellular loop, CCK$_A$-R(329−357), were incorporated into the model. NOE-restrained MD simulations were conducted for 500 ps in a membrane-mimetic solvent box composed of a lipophilic layer of decane sandwiched between two layers of water. Dihedral angle restraints were applied to the TM helices

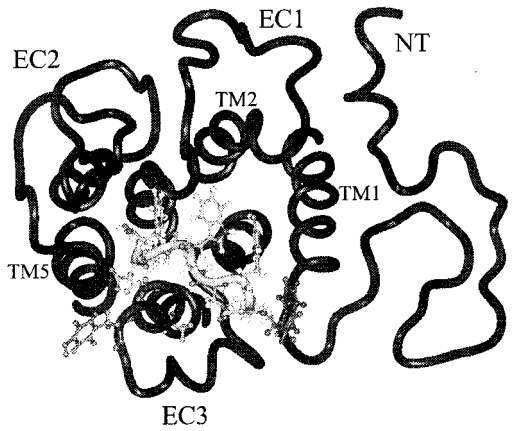

FIGURE 5: Molecular model of the CCK_A receptor and CCK-8 ligand following 500 ps of an NOE-restrained MD simulation in a water/decane/water membrane-mimetic solvent box. All of the residues of CCK-8 and the residues of CCK_A to which intermolecular NOEs were observed are depicted in ball-and-stick.

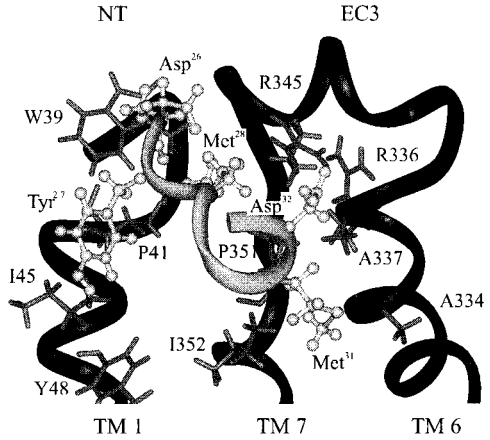

FIGURE 6: Expanded view of the interactions of CCK-8 (gray ribbon) with the N-terminus (NT) and third extracellular loop (EC3) of the CCK_A receptor (black ribbon). The side chains of the amino acids stabilizing the CCK-8/CCK_A ligand/receptor complex are illustrated as ball-and-sticks and sticks, respectively. The residues of the ligand are denoted using the three-letter code, those of CCK_A by the one-letter code.

during the initial phases of the simulation. The conformations and topological orientations of the N-terminus and third extracellular loop were consistent with those previously obtained for the receptor fragments (Figure 5). The disulfide-stabilized β-sheet of the N-terminus was closely associated with the water/decane interface, with its hydrophobic and hydrophilic side chains projected into the decane and aqueous phases, respectively. Residues adjoining the helical region between A341 and R346 in the third extracellular loop were in an extended conformation that projected the helix away from the TM bundle and parallel to the water/decane interface.

The ligand was placed in the extracellular aqueous phase of the solvent box, approximately 10 Å away from the NOE-generated intermolecular contact points between the ligand and the receptor fragments, CCK_A-R(1−47) and CCK_A-R(329−357). During the simulation, the ligand adopted an orientation that placed its pseudohelix parallel to the extracellular face of the TM bundle, with the N-terminus of CCK-8 directed toward TM1 and the C-terminus of CCK-8 directed toward TM6. A number of ligand/receptor interactions stabilizing the complex are observed (Figure 6). Electrostatic interactions include the side chain of Asp^{32} with R336 and R345 and a π-cation interaction between the amino terminus of Asp^{26} and the indole ring of W39. The side chain of Met^{31} is found in a hydrophobic pocket formed by A334, A337, and P351, while Met^{28} interacts with W39, P41, and P351. The side chain of Tyr^{27} is found in close proximity to W39, P41, I45, and Y48.

DISCUSSION

Through the use of NMR spectroscopy and computational chemistry, we have determined the structural features of the N-terminus, CCK_A-R(1−47), and the third extracellular loop, CCK_A-R(329−357), of the human CCK_A receptor. Given the importance of the extracellular domains for ligand binding, the structural preference of these domains is vital for the development of molecular models of the ligand/receptor complex. In the absence of the X-ray structure, our approach of examining receptor fragments (*32*), anchored to DPC micelles by inclusion of significant portions of the TM helices, is the only manner to obtain structural features of the extracellular (and cytoplasmic) domains of GPCRs. A number of features we have observed utilizing this approach for peptide GPCRs were found in the recent X-ray structure of rhodopsin (*33*). For example, we previously reported that the cysteine residue in the disulfide bond between the first and second extracellular loops is actually a turn and a half down in TM3 (*34*). The observation of a β-sheet in the far N-terminus of rhodopsin is in accord with our structure of the N-terminus of CCK_A-R (*14*).

In addition to the structural features of the extracellular domains, we also report the observation of a number of intermolecular NOEs between the receptor fragments and CCK-8. A titration of the receptor fragment with the ligand produces a specific interaction, which can be monitored by chemical shift perturbation and intermolecular NOEs. The intermolecular interactions are ligand-specific; utilization of other nonrelated ligands or scrambled peptides does not produce this effect (*14*). Indeed, nonspecific ligand/receptor interactions would not lead to NOEs. Interestingly, the NMR data indicate that the conformations of the ligand and receptor fragments are maintained during binding. These observations are consistent with the mechanism proposed by Schwyzer (*35*−*37*) and Moroder (*38*, *39*) for peptide hormone interactions with membrane-bound receptors. This model suggests that the ligand initially interacts with the cell membrane, whereby the ligand reorients from a random conformation to the bioactive conformation, prior to binding to the receptor.

The NOE-generated contact points between CCK-8 and CCK_A-R(329−357) place the C-terminus of the ligand in close proximity to TM6, in agreement with previously published mutagenesis data. Site-directed mutagenesis of the N333 and R336 residues in TM6, and the reciprocal mutations of Asp^{32} and the carboxamide of CCK established the importance of these residues in binding (*7*). The NOE-generated contact points were interdispersed in the same vicinity of the receptor, demonstrating the utility of this technique for the discernment of binding interactions. Photoaffinity studies with a radioiodinated analogue of CCK with Gly^{29} replaced with L-benzoylphenylalanine (Bpa) produced contact points with the H347 and L348 residues of rat CCK_A-R (*12*). According to the molecular model of the

receptor generated in the present study, Gly^{29} is indeed in close proximity to residues in the third extracellular loop.

Incorporating the structural features of CCK_A-R(1−47) and CCK_A-R(329−357) into a model of the CCK_A-R required only minor adjustments for merging the overlapping helical regions of the receptor fragments and transmembrane domains. The addition of the ligand to the model and extensive MD simulations indicated a preferred mode of ligand binding. The N-terminus of the ligand is found in close proximity with the extracellular portion of TM1, while the C-terminus of CCK-8 projects toward TM6. It is important to stress that the intermolecular NOEs between CCK-8 and receptor fragments can be simultaneously fulfilled with this mode of binding. Again this model is consistent with a number of reports, based on site-directed mutagenesis, in the literature (*7*, *10*). An alternative orientation of the ligand has been proposed, based on the finding of a contact point between *p*-NO_2-Phe^{33} of the modified ligand and W39 of the N-terminus of CCK_A-R (*11*). It should be noted that in the present study we do not observe NOEs between CCK_A-R(329−357) and the C-terminus of CCK-8 (Phe^{33}-NH_2), which based on our NMR examination is unstructured (*14*). Certainly, the replacement of the native Phe^{33} with *p*-NO_2-Phe can alter the ligand-binding mode, reducing the distance between the C-terminus of the ligand and W39 of CCK_A-R. Importantly, the NOE-derived contact points between CCK-8 and CCK_A-R(329−357) reported here are in perfect accord with the observed interaction between the carboxamide of CCK-8 and the N333 side chain (*10*). A similar binding mode, with the C-terminus of the hormone near TM6, has been developed from photoaffinity cross-linking studies for the binding of CCK-8 to CCK_B-R (*13*).

In summary, the computationally refined NMR structure of the third extracellular loop of CCK_A-R(329−357) and the observed intermolecular NOEs between the receptor fragment and CCK-8 were used to model the intermolecular interactions between CCK-8 and the CCK_A receptor. The experimental data were used to develop starting points for extensive MD simulations used to delineate important intermolecular interactions for ligand binding. This model differs from those previously reported in that it directly incorporates experimentally determined structural information for both the ligand and the receptor. Binding information derived in this manner was found to complement and augment binding information derived from site-directed mutagenesis and photoaffinity studies.

ACKNOWLEDGMENT

We thank Dr. Maria Pellegrini (BASF, Worcester, MA) for assistance with the research described here and preparation of the manuscript.

REFERENCES

1. Wank, S. A. (1995) *Am. J. Physiol. 269*, G628−646.
2. Silvente-Poirot, S., Dufresne, M., Vaysse, N., and Fourmy, D. (1993) *Eur. J. Biochem. 215*, 513−529.
3. Rehfeld, J. F., and van Solinge, W. W. (1994) *Adv. Cancer Res. 63*, 295−347.
4. Dunlop, J. (1998) *Gen. Pharmacol. 31*, 519−524.
5. Wank, S. A. (1998) *Am. J. Physiol. 274*, G607−613.
6. Sugg, E. E., Birkemo, L., Gan, L. S., and Tippin, T. K. (1998) *Pharm. Biotechnol. 11*, 507−524.
7. Kennedy, K., Gigoux, V., Escrieut, C., Maigret, B., Martinez, J., Moroder, L., Frehel, D., Gully, D., Vaysse, N., and Fourmy, D. (1997) *J. Biol. Chem. 272*, 2920−2926.
8. Gigoux, V., Escrieut, C., Silvente-Poirot, S., Maigret, B., Gouilleux, L., Fehrentz, J. A., Gully, D., Moroder, L., Vaysse, N., and Fourmy, D. (1998) *J. Biol. Chem. 273*, 14380−14386.
9. Gigoux, V., Maigret, B., Escrieut, C., Silvente-Poirot, S., Bouisson, M., Fehrentz, J. A., Moroder, L., Gully, D., Martinez, J., Vaysse, N., and Fourmy, A. D. (1999) *Protein Sci. 8*, 2347−2354.
10. Gigoux, V., Escrieut, C., Fehrentz, J. A., Poirot, S., Maigret, B., Moroder, L., Gully, D., Martinez, J., Vaysse, N., and Fourmy, D. (1999) *J. Biol. Chem. 274*, 20457−20464.
11. Ji, Z., Hadac, E. M., Henne, R. M., Patel, S. A., Lybrand, T. P., and Miller, L. J. (1997) *J. Biol. Chem. 272*, 24393−24401.
12. Hadac, E. M., Pinon, D. I., Ji, Z., Holicky, E. L., Henne, R. M., Lybrand, T. P., and Miller, L. J. (1998) *J. Biol. Chem. 273*, 12988−12993.
13. Anders, J., Bluggel, M., Meyer, H. E., Kuhne, R., ter Laak, A. M., Kojro, E., and Fahrenholz, F. (1999) *Biochemistry 38*, 6043−6055.
14. Pellegrini, M., and Mierke, D. F. (1999) *Biochemistry 38*, 14775−14783.
15. Delaglio, F., Grzesiek, S., Vuister, G. W., Zhu, G., Pfeifer, J., and Bax, A. (1995) *J. Biomol. NMR 6*, 277−293.
16. Braunschweiler, L., and Ernst, R. R. (1983) *J. Magn. Reson. 53*, 521−528.
17. Bax, A., and Davis, D. G. (1985) *J. Magn. Reson. 65*, 355−360.
18. Macura, S., Huang, Y., Suter, D., and Ernst, R. R. (1981) *J. Magn. Reson. 43*, 259−281.
19. Jeener, J., Meier, B. H., Bachmann, P., and Ernst, R. R. (1979) *J. Chem. Phys. 71*, 4546−4553.
20. States, D. J., Haberkorn, R. A., and Ruben, D. J. (1982) *J. Magn. Reson. 48*, 286−292.
21. Piotto, M., Saudek, V., and Sklenar, V. (1992) *J. Biomol. NMR 2*, 661−665.
22. Wuthrich, K., Billeter, M., and Braun, W. (1983) *J. Mol. Biol. 169*, 949−961.
23. Havel, T. F. (1991) *Prog. Biophys. Mol. Biol. 56*, 43−78.
24. Mierke, D. F., Scheek, R. M., and Kessler, H. (1994) *Biopolymers 34*, 559−563.
25. Pellegrini, M., Gobbo, M., Rocchi, R., Peggion, E., Mammi, S., and Mierke, D. F. (1996) *Biopolymers 40*, 561−569.
26. Berendsen, H. J. C., van der Spoel, D., and van Buuren, R. (1995) *Comput. Phys. Comm. 95*, 43−56.
27. Baldwin, J. M. (1993) *EMBO J. 12*, 1693−1703.
28. Baldwin, J. M., Schertler, G. F., and Unger, V. M. (1997) *J. Mol. Biol. 272*, 144−164.
29. Unger, V. M., Hargrave, P. A., Baldwin, J. M., and Schertler, G. F. (1997) *Nature 389*, 203−206.
30. Vriend, G. (1990) *J. Mol. Graph. 8*, 52−56.
31. McDonnel, P. A., and Opella, S. J. (1993) *J. Magn. Reson. B 102*, 120−125.
32. Pellegrini, M., and Mierke, D. F. (1999) *J. Pept. Sci. 51*, 208−220.
33. Palczewski, K., Kumasaka, T., Hori, T., Behnke, C. A., Motoshima, H., Fox, B. A., Le Trong, I., Teller, D. C., Okada, T., Stenkamp, R. E., Yamamoto, M., and Miyano, M. (2000) *Science 289*, 739−745.
34. Piserchio, A., Bisello, A., Rosenblatt, M., Chorev, M., and Mierke, D. F. (2000) *Biochemistry 39*, 8153−8160.
35. Schwyzer, R. (1991) *Biopolymers 31*, 785−792.
36. Schwyzer, R. (1992) *Braz. J. Med. Biol. Res. 25*, 1077−1089.
37. Schwyzer, R. (1995) *J. Mol. Recognit. 8*, 3−8.
38. Moroder, L., Romano, R., Guba, W., Mierke, D. F., Kessler, H., Delporte, C., Winand, J., and Christophe, J. (1993) *Biochemistry 32*, 13551−13559.
39. Moroder, L. (1997) *J. Pept. Sci. 3*, 1−14.

BI002659N